Applied Surface Science 661 (2024) 160082

Contents lists available at ScienceDirect

Applied Surface Science

journal homepage: www.elsevier.com/locate/apsusc

Full Length Article

Depth profiling of microwave nitrogen-terminated polycrystalline diamond surfaces by energy-dependent X-ray photoelectron spectroscopy

Arsène Chemin [a,*], Mohan Kumar Kuntumalla [b], Maria Brzhezinskaya [a], Tristan Petit [a], Alon Hoffman [b]

[a] Helmholtz-Zentrum Berlin für Materialien und Energie, Hahn-Meitner-Platz 1, 14109 Berlin, Germany
[b] Schulich Faculty of Chemistry, Technion-Israel Institute of Technology, Haifa 32000, Israel

ARTICLE INFO

Keywords:
Diamond
Nitrogen termination
Graphene-like islands
Nitrogen plasma
X-ray photoelectron spectroscopy
X-ray absorption spectroscopy
Depth profiling

ABSTRACT

Nitrogen-terminated diamonds hold promise for stabilizing near-surface NV^- centers, which is essential for reliable quantum sensing. Among various surface preparation methods, microwave (MW) nitrogen plasma, known for its minimal surface damage, appears as the most effective choice. In this investigation, we explore the nature of nitrogen bonding of polycrystalline diamond (PCD) surfaces exposed to MW nitrogen plasma using X-ray Photoelectron Spectroscopy (XPS) depth profiling and Near-Edge X-ray Absorption Fine Structure (NEXAFS) spectroscopy at the C *K*- and N *K*-edges. XPS depth profiling with atomic resolution, achieved by varying the probing photon energy using synchrotron radiation and supported by a physical model considering the associated inelastic mean free path, suggests a surface of almost fully saturated nitrogen in two main bonding configurations of similar contribution and a low coverage of ~5 % of graphene-like islands residing atop the nitrogen-terminated diamond surface. The thermal stability of these surface groups is monitored by *in situ* annealing up to 700 °C. The depth profiles reveal that nitrogen atoms do not diffuse in the diamond crystal, resulting in excellent diamond crystallinity in the first atomic planes below the surface. C *K*-edge NEXAFS analysis reveals the position of unoccupied surface states within the diamond bandgap, opening new perspective on the stabilization of near-surface NV^- centers.

1. Introduction

The control over the chemical and structural properties of diamond surfaces is of large importance for the emerging science and technology of quantum sensing using near-surface NV^- centers. It has been found that while surface defects and hydrogen termination of diamond surfaces have an adverse effect on NV^- population and measurement in the near-surface region of diamond, oxygen termination results in its enhancement [1,2]. On the other hand, nitrogen-terminated diamond surfaces may enhance the population of NV^- states through a combined effect of surface band bending and elimination of surface states in the band gap [3], a conclusion further supported by theoretical calculations [3]. From this perspective, it is also of large importance to be able to prepare a nitrogen-terminated diamond surface free of defects. The bonding of nitrogen in various configurations within the diamond matrix is relatively well understood from a structural, electronic, and optical properties point of view [4]. However, a detailed understanding of its interaction with diamond surfaces and near-surface regions is still in its infancy. This is due to the inherent difficulties associated with preparing structurally and chemically well-defined diamond surfaces. Surface nitridation processes require activation of the nitrogen molecule, which may cause irreversible changes to the diamond surfaces or near-surface structure. This is furthermore complicated by nitrogen co-adsorption with chemisorbed hydrogen, which naturally occurs on diamond surfaces prepared by standard chemical vapor deposition (CVD) methods and ambient exposure [5–7]. All these constraints may result in a multitude of nitrogen bonding configurations involving the interaction of nitrogen not just with the pristine diamond surface but also with local defects, hydrogen, oxygen, and other possible contaminants.

Recent studies combining X-ray photoelectron spectroscopy (XPS), ultraviolet photoelectron spectroscopy (UPS), low energy electron diffraction (LEED), and high-resolution electron energy loss spectroscopy (HREELS) have focused on the bonding and thermal stability of

* Corresponding author.
E-mail address: arsene.chemin@helmholtz-berlin.de (A. Chemin).

https://doi.org/10.1016/j.apsusc.2024.160082
Received 1 February 2024; Received in revised form 26 March 2024; Accepted 9 April 2024
Available online 10 April 2024

nitrogen with hydrogen-terminated (1 0 0) [8,9] and (1 1 1) [7,10] oriented single and polycrystalline diamond (PCD) [5,6] surfaces by exposure to radio frequency (RF) [5,8,10] and microwave (MW) [6,7,9] nitrogen plasmas. They revealed that nitrogen atoms may occupy various chemisorbed states, such as C-N/C═N and C≡N(nitrile-like), and induce positive electron affinity [5–10]. The lowest level of damage to the diamond near-surface region occurs upon MW(N_2) plasma exposure [6,7,9]. Regarding the nitrogen bonding configuration of the MW (N_2) PCD surfaces, the N (1s) XP peak was measured at 399 eV and was associated with bonding configuration defined by the C-N/C═N notation [6]. The full width at half maximum (FWHM) of this peak was measured to be ~1.8–1.9 eV after MW(N_2). Upon annealing, the N(1s) was found to decrease in intensity, mainly in the 500–700 °C range. From HREELS, there are two types of vibrational losses: C═N and CN-H_x bonds. The CN-H_x vibrational loss disappears upon annealing above 500 °C, and only C═N bonds remain. By comparing the decrease of the N(1s) peak intensity with annealing temperature, the amount of nitrogen bonded in these two bonding configurations is similar. From density functional theory (DFT) modeling, it has been shown that the CN bond length (without H) is 1.36 Å whereas the CNH bond length is 1.46–1.44 Å [11]. These bond lengths correspond to C═N and C-N "gas phase" bonding configurations. Therefore, it can be concluded that two different types of bonding configurations co-exist on the diamond surfaces upon MW(N_2), however, upon annealing above 500 °C, only the C═N remains on the surfaces.

Ex-situ LEED, XPS, and near-edge X-ray absorption fine structure (NEXAFS) studies demonstrated that, under well-controlled conditions, a nearly ordered surface was obtained, which is predominantly populated by C–N and C–H species [12] Thermal annealing experiments showed that nitrogen desorbs from the nitrided diamond surfaces over a wide temperature range (room temperature until 1000 °C), suggesting a heterogeneous bonding configuration of chemisorbed nitrogen differing from the case of well-defined NV center for which the thermal barrier for diffusion exceeds ~1200 °C [13]. Upon annealing to 1000 °C, the level of damage in the near-surface region of plasma nitrided diamond surfaces was found to be only partially removed [7]. We have recently optimized the MW(N_2) plasma conditions to produce highly ordered Di (1 0 0) [9] and Di(1 1 1) [7] nitrogen-covered surfaces. However, the presence and nature of local defects as well as the diffusion of nitrogen atoms within the first atomic layers of the diamond film remain open questions.

The use of synchrotron radiation to tune the excitation energy and, hence, the probing depth of XPS has been used to probe surface compositions of different surfaces, oxide layers, thin films, nanoparticles, nanotubes, etc. [14–21]. In contrast to angle resolved XPS, energy resolved XPS does not require a flat surface and can be used on PCD. For simple system, analytic models can be used to determine a profile [14–17]. The high surface sensitivity of XPS at low photoelectron kinetic energy (KE) was already employed to probe the surface groups of H-terminated diamond [22], but such a depth profiling of the first atomic planes has never been attempted on diamond to our knowledge.

In this study, a depth profile of the nitrogen bonding and local carbon defects in the first atomic planes of polycrystalline diamond after MW (N_2) plasma exposure, referred to as N-PCD, was achieved using XPS measured at different incident photon energies using a synchrotron X-ray light source. XPS at the C(1s) and N(1s) core levels of hydrogen-terminated polycrystalline diamond (H-PCD) after MW(N_2) plasma exposure and after *in situ* vacuum annealing the nitride surfaces to 300, 500, and 700 °C were acquired to investigate the thermal stability of the different adsorbed species and the related changes on the near-surface electronic structure. An analytical model was applied to fit the relative intensities of the C(1s) spectral components, allowing us to examine the depth distribution of the carbon species in the first atomic layers and determine the location of the sp^2 defects atop the pristine surface. A comparison with O-terminated and H-terminated Di(1 0 0) (O-Di(1 0 0) and H-Di(1 0 0)) and H-PCD surfaces allows the identification of specific nitrogen-related carbon bonding. In addition, a constant C(1s) and N(1s) photoelectron KE can be ensured, which allows a reliable quantitative estimation of the carbon and nitrogen contents on the surface. The XPS depth profiling is supported by NEXAFS spectroscopy, which is highly sensitive to the different carbon hybridization states and levels of disorder as well as to adsorbed species and sub-band gap electronic states. Furthermore, it allows for the determination of the energy of the unoccupied surface states within the bandgap of the diamond compared to the conduction band minimum, which may offer new insights on the stabilization role of nitrogen termination for sub-surface NV centers.

2. Experimental

PCD films: PCD films were grown onto p-type Si (1 0 0) substrates (10 × 10 mm^2) using H_2/CH_4 (99/1 vol%) gas mixture by hot filament CVD for 100 min in a system previously described [23]. The thickness of as-deposited PCD films was ~2–3 μm.

MW(N_2) plasma: The MW(N_2) plasma nitridation was accomplished by exposing the PCD surfaces to MW(N_2) plasma for 15 min. The N_2 flow rate, pressure, and MW power was maintained at 20 standard cubic centimeters per minute (sccm), 11 Torr, and 1000 W, respectively. During the MW(N_2) exposure, the estimated substrate temperature was ~120 °C. MW(N_2) plasma activation was achieved by inserting and activating hydrogen in the system at a dynamic flow rate of 250 sccm by the MW plasma source for 5 min, then high-purity nitrogen (99.9999 %) was introduced into the MWCVD chamber, and the hydrogen flow was discontinued. The MW system was leak tested to 10^{-3} Torr and dry pumps were used. The MW plasma nitridation was carried out at the Israeli Center of Advanced Diamond Technologies (ICDAT Ltd) using the MWCVD system (SEKI, 2.45 GHz, 6000 W). Following the MW nitridation process, the sample was transferred into ultrahigh vacuum (UHV) system at the HE-SGM beamline for NEXAFS and HR-XPS measurements under ambient conditions.

H-PCD: The H-terminated PCD surfaces were prepared by MW(H_2) plasma exposure. The H_2 flow rate, pressure, MW power, and the duration of the hydrogenation were 250 sccm, 90 Torr, 5000 W, and 20 min, respectively

H-Di(1 0 0): The hydrogen-terminated Di(1 0 0) surfaces (7 × 7 × 0.3 mm^3) were prepared by first exposure to an MW hydrogen plasma to remove any non-diamond carbon residues and any other possible contaminants from the surfaces. The H_2 flow rate, pressure, MW power, and the duration of the hydrogenation were 250 sccm, 90 Torr, 5000 W, and 20 min, respectively. Next, a short overgrowth of homo-epitaxial diamond layer (~1 μm) was carried out using CH_4 and H_2 as precursor gases at system pressure, substrate temperature, and flow rate of 140 Torr, 900 °C, and 10:250 sccm (CH_4:H_2), respectively, in MWCVD system (SEKI, 2.45 GHz, 6000 W) to heal any possible defects created by the polishing procedure and to ensure that the surfaces are well-defined and hydrogen-terminated. Details of this process were previously reported [7]. The surface preparation was carried out at ICDAT Ltd. This "healing" step is most important as MW hydrogen exposure and polishing may result in local defects, which will likely influence the bonding configuration and electronic properties of the diamond surfaces.

O-Di(1 0 0): The oxidized Di(1 0 0) surface was a 3 × 3 mm^2 × 250 μm boron-doped HPHT substrate (to avoid charging) with approximately 300 ppm (5 × 10^{19} atoms/cm^3). The oxidation was carried out by wet chemical treatment in a mixture of sulfuric acid and nitric acid (ratio 3:1) for 1.5 h at elevated temperatures. It was prepared by Dr. Peter Knittel from the Fraunhofer Institute for Applied Solid State Physics in Freiburg, Germany.

XPS and NEXAFS: The XPS and NEXAFS spectroscopic measurements were performed at the HE-SGM beamline of the electron storage ring BESSY-II at Helmholtz-Zentrum Berlin (Germany) using an ultrahigh vacuum (UHV) experimental station equipped with a Scienta R3000 electron energy analyzer (Scienta) [24]. Due to the HE-SGM optical scheme, carbon contamination is negligible on the beamline's optical

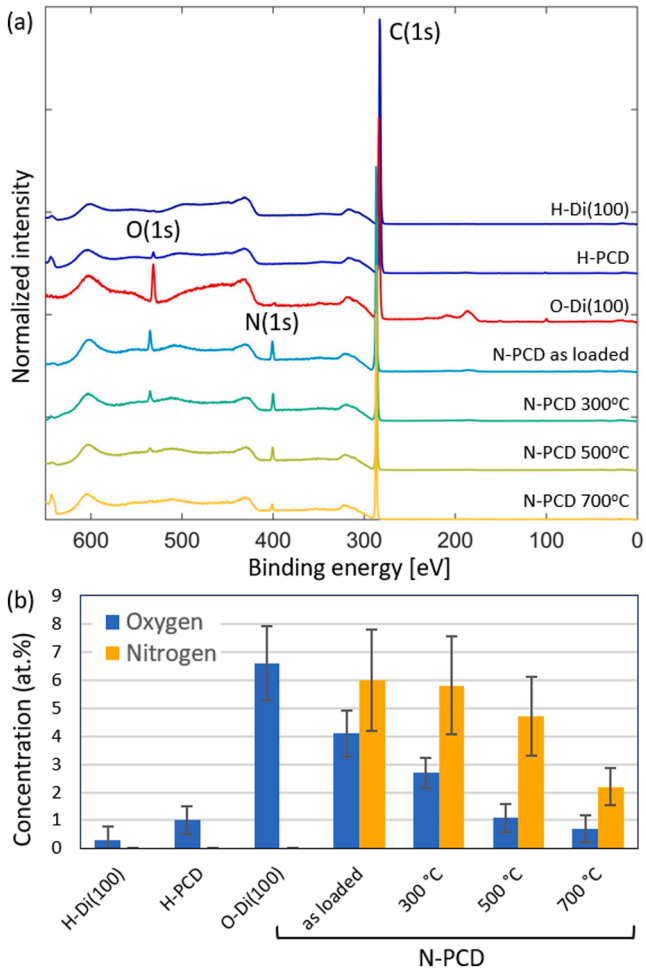

Fig. 1. (a) XPS surveys using an incident photon energy 700 eV for the H-Di (1 0 0), H-PCD, O-Di(1 0 0) and N-PCD, as loaded and after annealing to 300, 500 and 700 °C surfaces. (b) Calculated nitrogen and oxygen at.% as a function of annealing temperature from the XPS surveys measured for the different surfaces. Standard sensitivity factors of 1.0 for C, 1.8 for N, and 2.93 for O were used.

elements and no background correction is needed. The NEXAFS measurements were conducted in the total electron yield (TEY) mode, where the incident photon energy was swept and the emitted electrons from the sample were simultaneously recorded under a 30 V retarding potential. The spectra were normalized by the incident photon flux and between the pre-edge and post-edge regions. The energy resolution of the monochromator in the range of the C *K* X-ray absorption edges (~285 eV) was ~100 meV [25]. Combined with the hemispherical detection measuring conditions, the photoelectron energy resolution is better than 0.5 eV, which is estimated to be smaller than the natural width of the C(1s) and N(1s) core levels, resulting in XP lineshapes measurements of high chemical sensitivity compared to those obtained in our previous XPS studies [5,6].

Utilizing synchrotron radiation allowed us to vary the energy of the probing photons, thus changing the KE and mean free path of the inelastically scattered electrons and, consequently, probing different depths. The XPS surveys were performed using an incident energy of 700 eV. XPS measurements were performed at various incident photon energies either to match the C(1s), N(1s), and O(1s) photoelectron kinetic energies and thus equalize their mean free path and depth sensitivity or to probe different C(1s) information depths.

3. Results and discussion

3.1. XPS survey and atomic quantification

The surface chemical composition of the H-Di(1 0 0), H-PCD, O-Di (1 0 0), and N-PCD samples before annealing, referred to as 'as loaded' in the text and figures, and subsequently subjected to vacuum annealing at 300, 500, and 700 °C were measured by XPS (Fig. 1a). All XP spectra are dominated by an intense C(1s) peak centered at 285 eV for H-Di(1 0 0) and H-PCD, with slight upshifts observed on the O-Di(1 0 0) and N-PCD because of charging. The XPS of O-Di(1 0 0) and H-PCD also show an O (1s) peak at 532 eV. For the N-PCD surface, the XPS shows clear peaks at 532 eV, 400 eV, and 287 eV associated with O(1s), N(1s), and C(1s) photoelectrons. Upon annealing, both the O(1s) and N(1s) XP peaks decrease in intensity.

The calculated oxygen and nitrogen concentration in atomic percentage (at.%) derived from the XP spectra shown in Fig. 1a for the different samples and after annealing are displayed in Fig. 1b. Given that the distribution of oxygen and nitrogen within diamond is not homogeneous but localized at the surface, these values hold comparative significance only, as the probing depth is different for each KE.

The calculated oxygen concentrations of the O-Di(1 0 0), H-Di(1 0 0), and H-PCD surfaces are ~6.6, 0.3 at.%, and 1.0 at.% respectively, whereas the N-PCD surface displays an O concentration of ~4.1 at.% which monotonically decreases to ~2.7, ~1.1 and ~0.7 at.% upon annealing to 300, 500 and 700 °C, respectively. The larger oxygen concentration on the H-PCD surface than on the H-Di(1 0 0) surface is likely to be associated with the surface defects sites and grain boundaries promoting oxygen adsorption [26]. Similarly, the larger oxygen content on the N-PCD surface compared to the H-terminated surfaces is likely to be associated with some sp^2-defects at its surface, as later confirmed by XPS. Furthermore, the low thermal stability of the adventitious oxygen suggests that it is bonded to defective carbon sites [27]. It is coherent with the nature of the oxygen bonding on RF(N_2) and MW(N_2) plasma nitrided H-Di(1 0 0) surfaces as we recently reported [28]. Oxygen co-adsorption onto the nitrogen-terminated H-Di(1 0 0) surfaces from uncontrolled ambient containing molecules has been recently reported [28]. The level of oxygen adsorption is influenced by the level of surface defects during the nitridation process [28]. From the O(1s) BE position, it was determined in that study that oxygen is weakly bonded to the diamond surface, forming CO_x bonds and does not form NO_x bonds [28].

3.2. XPS core levels and bonding configuration

To further elucidate the nature of the nitrogen bonding to the surface, the C(1s), N(1s) and O(1s) XP spectra were measured using photon energies of 335, 450, and 580 eV, respectively, as presented in Fig. 2. The photoelectron KE using these photon energies is ~50 eV for the three atoms, resulting in a similar inelastic mean free path of ~5 Å [29].

Whilst some global shifts in the BE were measured for the different samples, likely associated with small homogeneous charging and band bending, the BE of the main C(1s) peak was positioned at 285.0 eV for all surfaces in Fig. 2a. As observed from Fig. 2a, spectral deconvolution of the C(1s) XP line measured for the H-Di(1 0 0) shows that it is clearly composed of two peaks at 285.0 and 285.8 eV with FWHM of 0.5 and 0.9 eV, respectively. The 285.0 eV component is associated with C–C bonds in the diamond matrix and, therefore, associated with sp^3-bonded carbon, whereas the 285.8 eV component is associated with carbon atoms bonded to hydrogen on the diamond surface [22,30]. The larger FWHM measured for the latter is probably associated with the fact that hydrogen may be bonded on the diamond surface in more than one hydrogen bonding configuration to the H-Di(1 0 0) surface (i.e., CH and CH_2). Evidence that more than one hydrogen bonding configuration occurs on the H-D(1 0 0) surface was obtained from HREELS of similarly prepared surfaces [7]. No other contributions to the C(1s) XP line shape were measured, suggesting the level of defects on this surface was very

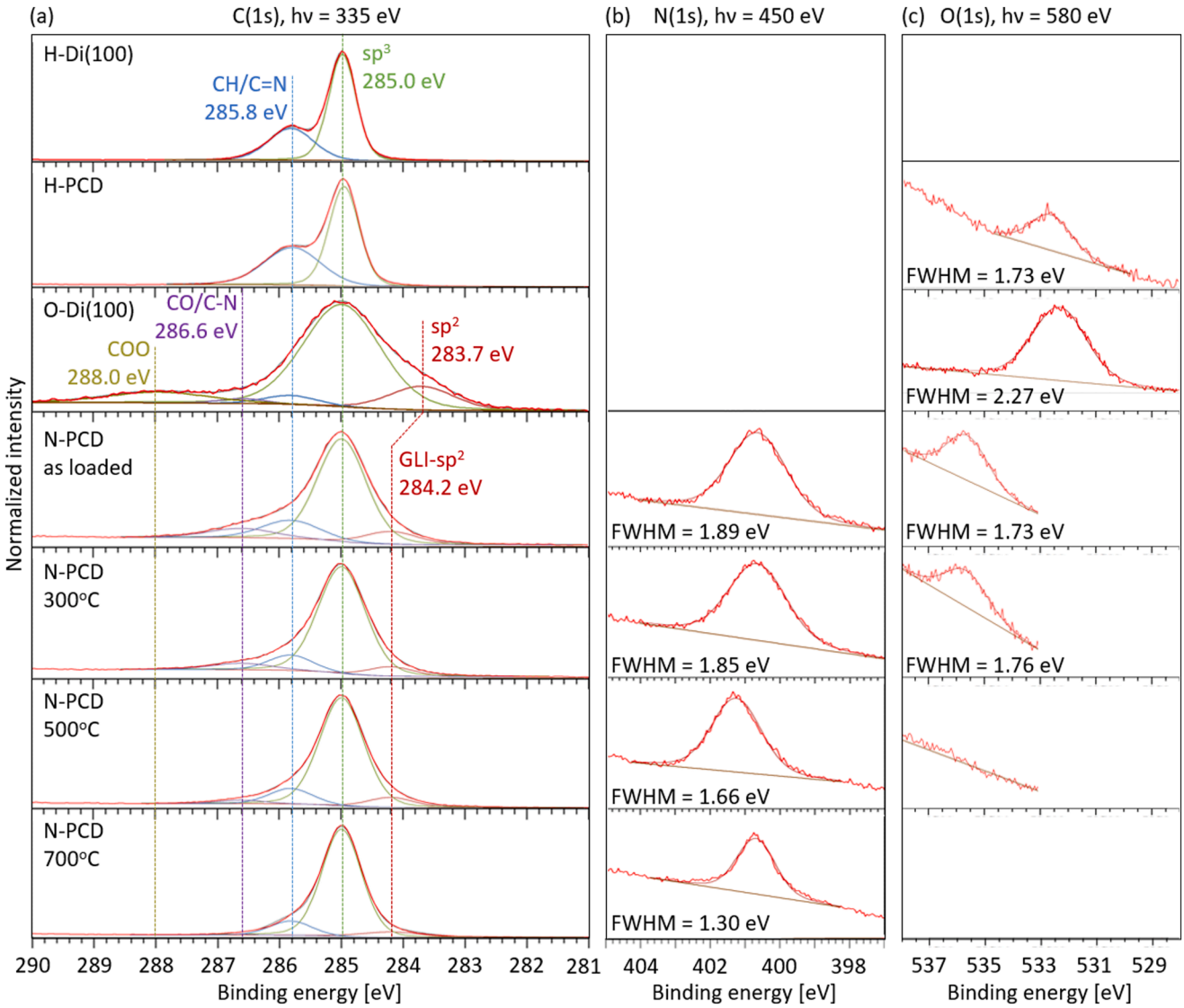

Fig. 2. (a) C(1s) XP line shapes measured at an incident photon energy of 335 eV for the H-Di(1 0 0), H-PCD, O-Di(1 0 0) and N-PCD surface and after annealing to different temperatures. The spectra are shifted such that the C(sp^3) appears at 285.0 eV. (b) N(1s) XP line shapes measured at an incident photon energy of 450 eV for the N-PCD and after annealing to different temperatures. (c) O(1s) XP line shapes measured at an incident photon energy of 580 eV for the H-PCD, O-Di(1 0 0), N-PCD surface and after annealing to different temperatures.

low.

Deconvolution of the C(1s) XP lineshape measured for the H-PCD sample shows that it is also composed of two peaks centered at 285.0 and 285.8 eV, similar to the H-Di(1 0 0), but the peaks are slightly broader with an FWHM of 0.6 eV for the sp^3-bonded carbon and 1.05 eV for the CH. It is coherent with the fact that the H-PCD surface possesses an increased amount of crystal defects and exposes different crystal orientations ((1 0 0), (1 1 0), and (1 1 1)) and grain boundaries, leading to a larger possibility of hydrogen bonding resulting in the observed broadening.

For the O-Di(1 0 0) surface, the C(1s) XP line shape could be deconvoluted into several spectral components at: 288.0, 286.6, 285.8, 285.0, and 283.7 eV associated with C═O, C-O, C–H, C–C(sp^3) and C═C(sp^2) (related to defects) bonded carbon, respectively [31]. In particular, the appearance of the 283.7 eV spectral component suggests that the oxidation process is accompanied by the formation of a disordered carbon layer, as previously reported by us and others [31,32]. The assignment of these chemical states is supported by HREELS for which similar chemical states were measured for the oxidized PCD surfaces by an acid treatment and vibrational losses associated with C-O, C═O, and sp^2-bonded carbon were measured [31]. This agrees with the spectral analysis of the C(1s) XP lineshape measured for the O-Di(1 0 0) above. For the O-Di(1 0 0), the FWHM of the C(sp^3) bonded carbon was 1.46 eV. The larger FWHM value measured in this case compared to the H-Di (1 0 0) surface is due to the disorder induced by the oxidation process and the possibility of oxygen diffusion into the sub-surface region of diamond.

The C(1s) XP lineshape measured after exposure to the MW(N_2) plasma shows some significant differences as those compared to the O-Di (1 0 0), H-PCD, and H-Di(1 0 0), which served as references in this study. The spectral component associated with sp^2 carbon defects was measured at 284.2 eV compared to 283.7 eV for the oxidized surface. Such a reduction of the difference in energy with the C(sp^3) suggests that this component is not related to defect induced by the surface termination like for O-Di(1 0 0) but rather some graphene-like island (GLI) created at the surface of N-PCD. Such defects consist of graphene-like structures atop the surface of the diamond and have been previously observed on nanodiamonds and boron-doped diamonds [33,34]. This observation is confirmed by the NEXAFS measurements and the depth profile model on the energy-dependent XPS presented later. In addition,

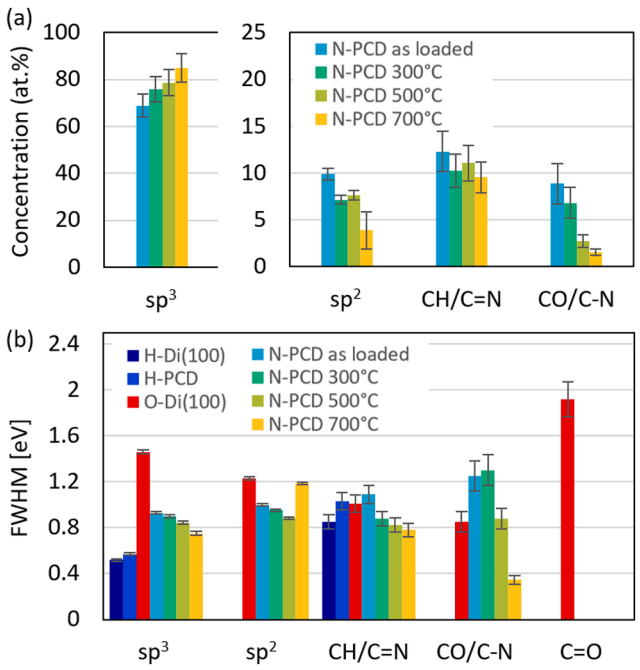

Fig. 3. Spectral analysis of the C(1s) and N(1s) XP lines shown in Fig. 2. (a) Evolution of the relative concentration (at.%) of different spectral components of the C(1s) XP peak on the N-PCD with the annealing temperature. (b) FWHM of the C(1s) spectral components for different surfaces.

spectral components were measured at 285.8 and 286.6 eV associated with CH/C═N and CO/C-N bonds, respectively. No spectral component at 288.8 eV associated with C═O bonds was measured.

As shown in Fig. 3a, after annealing to 300, 500, and 700 °C, the C (1s) XP spectral relative intensity of components associated with CO/C-N bonding and GLI-sp^2 carbon decreased in intensity, whereas those associated with C(sp^3) increased and the CH/C═N component remained nearly constant (within the statistical error of our analysis). These results agree with the decrease of nitrogen and oxygen calculated from the XPS surveys and shown in Fig. 1b. No changes in the CH concentration are expected within the annealing temperature of our experiments. This agreement supports the assignment of the different spectral components of the C(1s) XP line and shows the chemical completeness of our analysis. The FWHM of the different C(1s) spectral components following MW(N_2) exposure and annealing are summarized in Fig. 3b. The FWHM of the C(1s) spectral component associated with sp3-bonded carbon (i.e., at 285.0 eV) is ~1.5 eV larger (1.5 eV instead of 1.0 eV) than that measured for the H-PCD surfaces. This increase in the FWHM is associated with the influence of the nitrogen bonding through a secondary effect.

The N(1s) XP peak, shown in Fig. 2b, measured after the MW(N_2) plasma termination and annealing to the different temperatures, displayed a symmetric line shape and was centered at 400.65 eV. With annealing temperature, this peak intensity decreases due to desorption of nitrogen. The FWHM of the N(1s) peak obtained a value of 1.89, 1.85, 1.66, and 1.33 eV following MW(N_2) exposure and after annealing to 300, 500 and 700 °C, respectively. The decrease in FWHM suggests that nitrogen is bonded to the diamond surface in more than one bonding configuration and that with annealing, preferred desorption of a particular bonding configuration occurs, resulting in the population of a particular bonding state [6,7,9]. Also, from Fig. 3a, upon annealing, there is a preferential decrease of the CO/C-N and C═C(sp^2) (defects) components as opposed to that associated with CH/C═N, suggesting that the C═N bonding configuration is more thermally stable than the others.

The possibility that the narrowing of the N(1s) peak is attributed to the preferential desorption of a particular nitrogen bonding nitrogen species is further supported by HREELS measurements, which showed that N-PCD surface in the 500–700 °C range, as in the present study, a vibrational loss attributed to NH_x species disappear from the loss spectrum [6]. Furthermore, TPD measurements showed that in this temperature range, HCN species desorbed from the surfaces [5].

The N(1s) XP lineshape shows that nitrogen is not bonded to defect sites or to the GLI but that it is mostly bonded to surface diamond atoms in support of our previously reported measurements [6]. As no high BE component was measured to the N(1s) XP peak that may be associated with nitrogen bonding to oxygen, it may be concluded that the adventitious oxygen measured in the XPS survey does not form NO_x-type surface bonds but is directly bonded to the diamond surface or GLI-sp^2 as discussed above.

3.3. Energy resolved XPS and depth profiling

To delve deeper into the surface and sub-surface characteristics of the nitride layer, we conducted C(1s) XP peak measurements while varying the incident photon energy, hence the photoelectron KE and, in turn, the depth sensitivity of the measurements [19]. Measurements carried out for the nitride surfaces are shown in Fig. 4a using photon energies of 335, 435, 535, and 700 eV, resulting in C(1s) photoelectron KE of 50, 150, 250, and 415 eV, respectively. The difference in kinetic energies due to the difference of BE for the different carbon configurations is negligible for a given excitation photon energy. The evolution of the C(1s) XP line shape and spectral components with excitation energy is due to the increase in the photoelectron inelastic mean free path (IMFP) with increasing KE, resulting in a decreased contribution of photoelectrons originating from the upper surface. The relative intensities of the C(1s) XP spectral components derived from the spectra measured on N-PCD are shown in Fig. 4b. The relative percentage of the C(sp^3) spectral component clearly increases with the incident photon energy and confirms it originates from the bulk diamond. On the contrary, the remaining spectral component noticeably diminishes as the photon energy increases, confirming its surface origin. No carbon bonded with nitrogen component is observed increasing. This provides evidence that the nitrogen atoms introduced into the diamond lattice through this surface treatment are substantially fewer in number compared to those in the terminal positions.

To compute the relative atomic percentages of each population of atoms (sp^3, sp^2, and those bonded to terminal atoms), the number of photoelectrons emitted from each population that are detected by the analyzer is calculated. This number depends on the proportion of each population, but also on the depth of these atoms and the energy of the incident photon through the absorption and emission cross-sections.

The number of photoelectrons N detected from a C atom can be calculated based on Beer-Lambert law in our geometry. It decreases exponentially with its distance d to the surface as more and more photoelectrons are inelastically scattered:

$$N \propto N_0 e^{-\frac{d}{\lambda(K)\cos(\alpha)}}$$

with N_0 the number of photoelectrons emitted, $\lambda(K)$ the inelastic mean free path (IMFP), K the KE of the photoelectron, and α the angle between the surface normal and the detector axis. The PCD surface is not flat to the atomic level, but on average, $\alpha = 45^o$. As a first approximation, the IMFP $\lambda(K)$ is independent of the nature of the solid [29]:

$$\lambda(K) = \frac{143}{K^2} + 0.054\sqrt{K} \text{ with } K = E - 285eV$$

The number of photoelectrons emitted, N_0, is proportional to the cross-sections of absorption and emission of the C atom, depending on the photon energy E and the photon flux. The photon flux can be considered constant over the depth of the sample as the absorption depth of an X-ray photon is much larger than the IMFP of the detected electron.

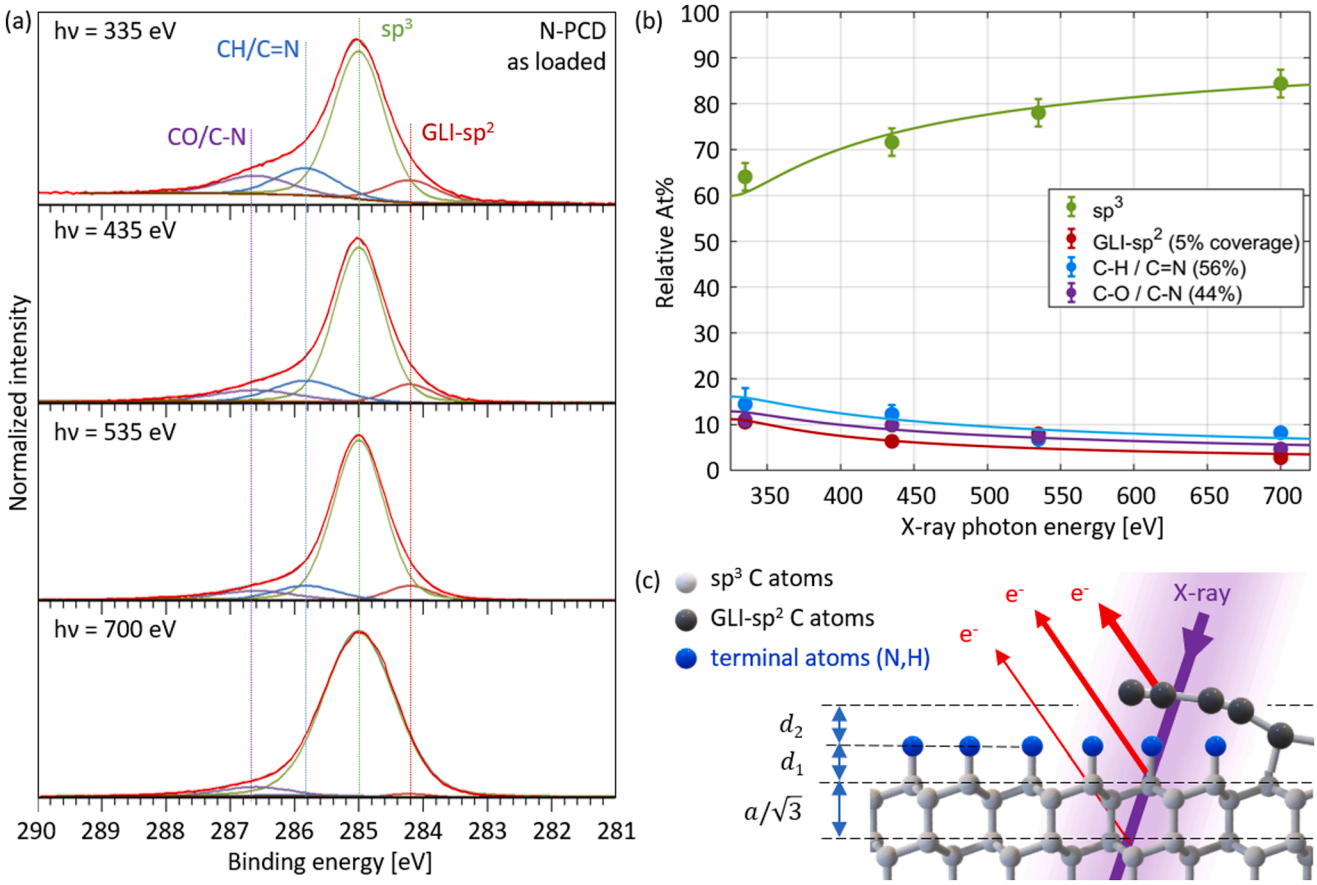

Fig. 4. XPS depth analysis. (a) C(1s) XP lines shape measured as a function of incident photon energy for the as-MW(N_2) exposed PCD surface as loaded. (b) Calculated relative concentration (at.%) of the C(1s) XP spectral components measured as a function of incident photon energy for the N-PCD surface (from spectra shown in panel (a)). (c) Cross-section of the system considered by the model consisting of a (1 1 1) diamond surface terminated by N atoms and partially covered by GLI.

To obtain the total number of photoelectrons detected for a given bonding configuration X, one needs to sum the components coming from all the C atoms in the bonding configuration X, depending on their depth from the surface d:

$$I_X = \sum N_X(d,E) \propto \sum N_{X,0}(E) e^{-\frac{d}{\lambda(E)\cos(\alpha)}}$$

To do so, a geometrical model of the surface and bulk has to be assumed to calculate d. The model chosen here is given in Fig. 4c and discussed further later.

$N_{X,0}(E)$ takes into account the photon flux and cross-sections depending only on E. The relative concentration (at.%) of C in a bonding configuration X is given by:

$$I_X(E) = \frac{I_X}{\sum_X I_X}$$

From the previous equation, $N_{X,0}(E)$ simplifies so that the relative concentration (at.%) can be computed for the different energies only considering the IMFP and the position of the atoms.

The evolution of the relative atomic percentage for each component of the C(1s) spectrum presented in Fig. 4b was simulated using a model of an ideal diamond, as shown in Fig. 4c, with a (1 1 1) surface, featuring terminal atoms (depicted in blue), and partial coverage by GLI. The specific identity of these terminal atoms and their bonding configurations are not explicitly defined within the model. They may also represent multi-atomic groups like N–H or O–H, provided they do not contain carbon atoms. These terminal atoms could be singly bonded to a carbon atom, such as H, or form a bridge between two surface carbon atoms, such as N–H. In the latter case, both carbon atoms are treated as having the same terminal atom and are considered equivalent. Hence, the model simplifies the carbon atom populations into two distinct categories, corresponding to the previous XPS analysis: one for the CH/C═N peak and another for the CO/C-N peak. For a more comprehensive discussion regarding the precise nature of these components, please refer to the earlier discussions. It is expected that the N-PCD consists of both (1 0 0) and (1 1 1) surfaces, although the (1 1 1) surface is anticipated to be the predominant one [35]. We have performed detailed modeling to validate this hypothesis, and we found that a model considering a (1 0 0) surface does not align well with the experimental (see supplementary information). The presence of a GLI on top of the surface is substantiated by the XPS BE data, as explained earlier, and further supported by NEXAFS measurements, as discussed later. Considering that the C(1s) spectral component associated with sp^2-hybridized carbon was measured at 284.2 eV, ~0.4 eV larger BE than that measured for the O-terminated diamond surface and that produced by low-energy Ar^+ irradiated diamond surface [35], it is argued that this graphitic layer possesses in fact a graphene-like nature. Furthermore, a model solely based on surface reconstruction induced by missing terminal atoms does not accurately replicate the experimental data, as demonstrated in the SI. Note that such a low surface coverage of GLI-sp^2 carbon cannot be detected with lab-based XPS as this contribution is hardly visible at 700 eV excitation.

The distance of each atom relative to the surface is computed from the geometry described in Fig. 4b, considering a partial coverage by sp^2-hybridized carbon. The distance $d_1 = 0.15$ nm is optimized on a model without graphene (see SI). It appears to be in good agreement with the

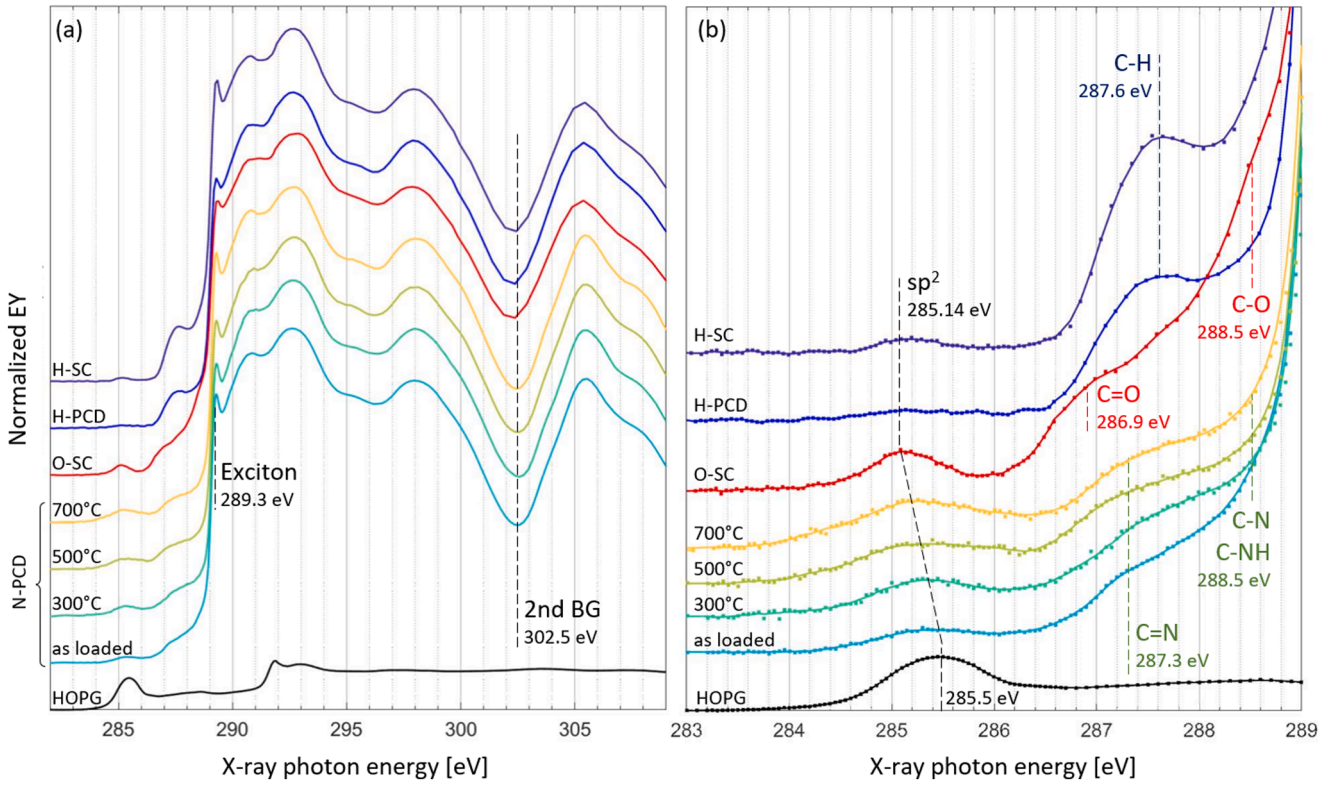

Fig. 5. (a) C *K*-edge NEXAFS spectra of the different surfaces: H-Di(1 0 0), H-PCD, O-Di(1 0 0), HOPG, N-PCD as-loaded and after annealing to different temperatures. All the spectra are normalized between the pre-edge and the post-edge regions. (b) Zoom on the pre-edge region.

theoretical calculation of nitrogenated surfaces previously reported [11]. The distance $d_2 \sim$ nm is estimated from similar structures observed by TEM or STM on nanodiamonds [36] and boron-doped diamonds [34]. The model is little sensitive to this distance as the graphitic coverage of the surface is limited. The (1 1 1) interatomic layer in the diamond is $a/\sqrt{3}$ with $a = 0.3567$ nm (lattice parameter). The atomic surface density of the (1 1 1) diamond plan is $\frac{4}{a^2\sqrt{3}} = 18.15\ \mathrm{nm}^{-2}$ while the atomic surface density of the GLI is taken as the one of graphene 38.2 nm^{-2}. In the case of the (1 1 1) surface, only half of the surface C atoms are bonded to terminal atoms. The others are equivalent to bulk sp^3 atoms.

Considering the atomic surface density of individual layers and their respective distances from the surface enables the calculation of the relative number of photoelectrons detected for each bonding configuration of carbon atoms, thereby the determination of the relative atomic percentages (at.%). This model is then fitted on the experimental data using a nonlinear curve fitting algorithm considering only three fitting parameters: the fraction of the surface covered by GLI, the fraction of CH/C═N and CO/C-N bonds at the surface of the diamond. An example of the full code is provided in the SI.

It appears that before annealing, about 56 % of the surface bonds are CH/C═N while 44 % are CO/C-N and the GLI covers only 5 % of the surface. After annealing at 700 °C, all the CO/C-N are desorbed, as well as a part of the CH/C═N bonds decreasing to only 34 % of the surface atoms (see SI). Similarly, about half of GLI desorbs and the remaining coverage is only 3 %. These results are in agreement with our previously published HREELS studies [6]. Upon MW(N_2) of H-PCD, a pronounced peak corresponding to ν(C═C) was observed at 170–180 meV loss energy, which disappears with annealing temperature: it decreases upon annealing to 500 °C and completely disappears upon annealing to 700 °C. This result was puzzling: usually, the opposite occurs: defective carbon structures anneal into a graphitic structure. The mechanism of formation of these islands by MW(N_2) exposure is under investigation by our team at the present time.

The altered configuration of carbon atoms resulting from the removal of terminal atoms with annealing does not produce a distinct peak but seems to add to the sp^3 component and are likely to remain dangling bonds. Considering the resolution of the measurement, it is impossible to distinguish them properly. The shift from graphitic sp^2 to surface sp^2 due to the annealing is, however, observed in NEXAFS.

3.4. NEXAFS measurements

C *K*- and N *K* NEXAFS spectra for the H-Di(1 0 0), H-PCD, O-Di(1 0 0), N-PCD surfaces as loaded and and after annealing to 300, 500, and 700 °C and highly oriented pyrolytic graphite (HOPG) are shown in Fig. 5a. The sharp peak at 289.3 eV is associated with transitions to the core exciton of the diamond crystal, while the strong dip at 302.5 eV is associated with the 2nd bandgap of the diamond. Most interesting are the features in the pre-edge region, below the exciton, corresponding to the absorption of unoccupied surface states.

From Fig. 5b, the pre-edge structure of H-Di(1 0 0) and H-PCD is dominated by an absorption peak at 287.6 eV associated with CH bonding on the diamond surface [37]. In addition, a lower intensity and broad peak is observed at 285.14 eV associated with C═C(sp^2) (related to defects) on the H-terminated diamond surface or sub-surface region. The pre-edge C *K*-edge NEXAFS of the O-Di(1 0 0) surface shows a few peaks corresponded to C═C(sp^2) at 285.09 eV [38,39]. C═O at 286.9 eV [40], and C-O at 288.5 eV [41]. It is interesting to note that the oxidation processes result in defects on the diamond surfaces with an absorption of 0.4 eV lower than the absorption of the HOPG sp^2 carbon (as indicated by the dashed line in Fig. 5b. This can be seen by both NEXAFS and C(1s) XP line shape analysis presented above.

The C *K* pre-edge NEXAFS of the N-PCD surface reveals a broad peak at 285.40 eV, reminiscent of HOPG, which shifts towards 285.2 eV upon annealing. In conjunction with previous XPS observations, the initial peak at 285.40 eV likely originates from the GLI atop the diamond, while

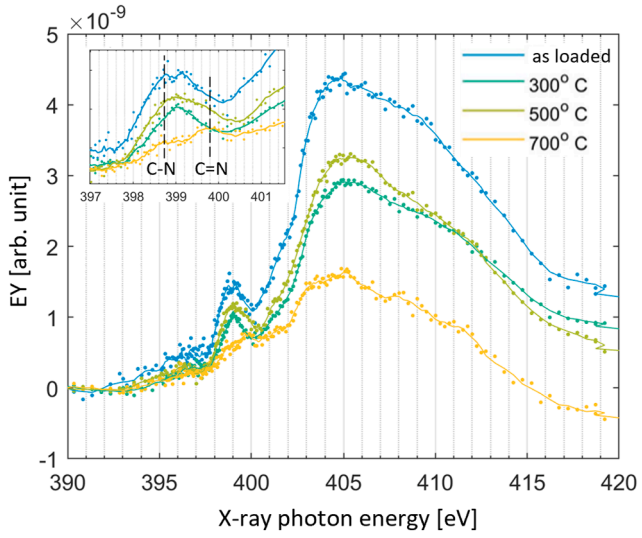

Fig. 6. N(1s) NEXAFS spectra of N-PCD as-loaded and after annealing to different temperatures.

the nitrogenated surface displays relatively few defects. With annealing, a portion of the graphitic layer desorbs, along with terminal atoms, resulting in local relaxation and reconstruction. A similar effect occurs upon adsorption of hydrogen from diamond surfaces. The shift toward 285.2 eV appears to stem from the surface reconstruction of the diamond.

The C *K*-edge of the N-PCD sample also exhibits a broad shoulder at 287.3 eV that we attribute to C═N bonding configuration as it appears stable during annealing. The second shoulder at 288.5 eV is attributed to C-O/C-N bonds as it desorbs with annealing. After annealing at 300 °C, one can observe a strong decrease above 288 eV, corresponding to the desorption of C-O/C-N bonds. One can observe an increase of the absorption around 285 eV corresponding to the sp^2 surface reconstruction discussed previously.

This attribution of bonding configuration is confirmed by the N *K*-edge NEXAFS. Fig. 6 shows the NEXAFS measured for the N-PCD surfaces as loaded and after annealing to 300, 500, and 700 °C. They are composed of a main edge around 405 eV and a pre-edge structure below 400 eV. In contrast to the C *K*-edge, here the spectra are not normalized but simply overlayed. Overall, the amplitude of the signal decreases with the annealing temperature due to the progressive N desorption. The inset presents a zoom on the pre-edge structures where two components can be identified, confirming the XPS and C *K*-edge analysis. One at 398.8 eV, attributed to C-N bonds because it is strongly reduced upon annealing. The second one at 399.8 eV, attributed to C═N bonds because of its higher thermal stability.

The position in energy of the surface states within the bandgap can be determined for the C *K*-edge NEXAFS. The core exciton at 289.3 eV is used to determine the CB minimum of the diamond by adding the energy of the core exciton measured elsewhere (~0.19 eV) [42], as we previously demonstrated [43]. Unoccupied surface states in diamonds can be involved in charge transfer and charge trapping [43]. The nitrogen termination C═N and C-N states are energetically higher than C═O and sp^2 defects and thus can improve the stability of the NV^- centers by reducing the possible trapping states. In particular, one can observe that the C═O and C═C(sp^2) (related to defects) surface states, present on the oxidized surface, lie below the $^3A_2$ energy level of the NV^- center. In the case of shallow implantation, these surface states can hinder the charge stability of the NV^- center due to charge trapping. Conversely, the C═N energy state determined here lies above the $^3A_2$ energy level, limiting potential trapping. Furthermore, the good quality of the surface termination also limits C═C(sp^2) related to surface defects, while the GLI-sp^2 is further localized, limiting charge transfers. A schematic representation of the different unoccupied levels discussed is shown in Fig. 7.

4. Conclusion

This investigation into the surface states obtained by MW(N_2) plasma treatment on polycrystalline diamond surfaces has unveiled significant insights crucial for the stability of near-surface NV^- centers. The MW (N_2) plasma treatment has proven highly effective, yielding a clean and surface fully covered with nitrogen with limited sp^2 surface defects. Sp^2 carbon mainly corresponds to GLI atop the diamond surface and is not identified in the further atomic layers. It holds promise for the creation and charge stability of shallow NV^- centers essential for quantum sensing applications. The depth profiling allowed by XPS at varying excitation energies has enabled a comprehensive examination of the surface structure. The presence of two distinct nitrogen bonding configurations, specifically C-NH and/or C-N, and C═N, in nearly equal proportions on the top diamond layer is evidenced. Upon annealing at 500 °C, one of the configurations, C-NH and/or C-N, undergoes desorption, leading to surface reconstruction and the formation of dangling bonds. However, the other configuration, C═N, remains mostly stable even at elevated temperatures up to 700 °C. A modeling of the depth profiling considering the IMFP of the photoelectron is proposed to validate the atomic structure of the near-surface region. The XPS depth profiling methodology described here may be extremely valuable to probe chemical bonding configuration with atomic sensitivity in other surfaces, thin films or interfaces involving 2D materials.

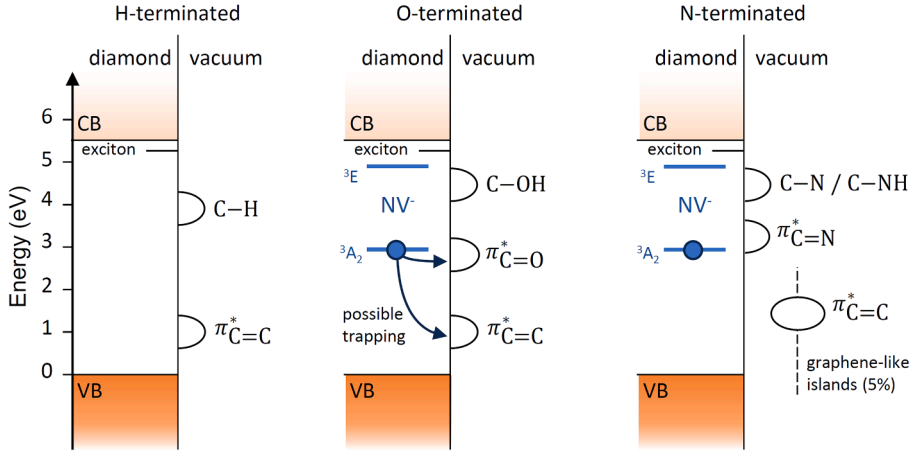

Fig. 7. Position of the unoccupied surface states within the bandgap determined by NEXAFS measurements and potential charge trapping mechanism of NV centers.

CRediT authorship contribution statement

Arsène Chemin: Writing – review & editing, Writing – original draft, Methodology, Investigation, Formal analysis, Data curation. **Mohan Kumar Kuntumalla:** Investigation, Data curation, Writing – review & editing. **Maria Brzhezinskaya:** Data curation, Resources, Validation, Writing – review & editing. **Tristan Petit:** Writing – review & editing, Supervision, Resources, Project administration, Methodology, Investigation, Conceptualization. **Alon Hoffman:** Supervision, Resources, Project administration, Methodology, Investigation, Funding acquisition, Data curation, Conceptualization, Writing – original draft, Writing – review & editing.

Declaration of competing interest

The authors declare that they have no known competing financial interests or personal relationships that could have appeared to influence the work reported in this paper.

Data availability

Data will be made available on request.

Acknowledgements

We would like to thank Dr. Peter Knittel for providing the oxidized single crystal diamond used as a reference in this work. This work is funded by a Freigeist Fellowship from the Volkswagen Foundation (n° 89592). A.C. and T.D. are grateful to BMWi for financial support (KK5085302DF0). A.H. and M.K.K would like to thank Technion-IIT for the promotion of research. This research was supported by the ISRAEL SCIENCE FOUNDATION (Grant No. 557/23). We would also like to thank Helen Diller Quantum Center, Technion, for the financial support to carry out this work. We thank Helmholtz-Zentrum Berlin (HZB) for the allocation of synchrotron radiation beamtime at HZB (Germany).

Appendix A. Supplementary data

Supplementary data to this article can be found online at https://doi.org/10.1016/j.apsusc.2024.160082.

References

[1] A. Stacey, T.J. Karle, L.P. McGuinness, B.C. Gibson, K. Ganesan, S. Tomljenovic-Hanic, A.D. Greentree, A. Hoffman, R.G. Beausoleil, S. Prawer, Depletion of nitrogen-vacancy color centers in diamond via hydrogen passivation, Appl. Phys. Lett. 100 (2012) 071902.
[2] M. Kim, H.J. Mamin, M.H. Sherwood, C.T. Rettner, J. Frommer, D. Rugar, Effect of oxygen plasma and thermal oxidation on shallow nitrogen-vacancy centers in diamond, Appl. Phys. Lett. 105 (2014) 042406.
[3] J.-P. Chou, A. Retzker, A. Gali, Nitrogen-terminated diamond (111) Surface for room-temperature quantum sensing and simulation, Nano Lett. 17 (2017) 2294–2298.
[4] M.N.R. Ashfold, J.P. Goss, B.L. Green, P.W. May, M.E. Newton, C.V. Peaker, Nitrogen in diamond, Chem. Rev. 120 (2020) 5745–5794.
[5] M.K. Kuntumalla, M. Attrash, F. Li, A. Hoffman, Influence of RF(N2) plasma conditions on the chemical interaction and stability of activated nitrogen with polycrystalline diamond surfaces: a XPS, TPD and HREELS study, Surf. Sci. 679 (2019) 37–49.
[6] M. Attrash, M.K. Kuntumalla, S. Michaelson, A. Hoffman, Nitrogen-terminated polycrystalline diamond surfaces by microwave chemical vapor deposition: thermal stability, chemical states, and electronic structure, J. Phys. Chem. C 124 (2020) 5657–5664.
[7] M.K. Kuntumalla, Y. Zheng, M. Attrash, G. Gani, S. Michaelson, K. Huang, A. Hoffman, Microwave N2 plasma nitridation of H-diamond (111) surface studied by ex situ XPS, HREELS, UPS, TPD, LEED and DFT, Appl. Surf. Sci. 600 (2022) 154085.
[8] M. Attrash, M.K. Kuntumalla, A. Hoffman, Bonding, structural properties and thermal stability of low damage RF (N2) plasma treated diamond (100) surfaces studied by XPS, LEED, and TPD, Surf. Sci. 681 (2019) 95–103.
[9] Y. Zheng, M.K. Kuntumalla, M. Attrash, A. Hoffman, K. Huang, Effect of Surface hydrogenation on the adsorption and thermal evolution of nitrogen species on Diamond(001) by microwave N2 plasma, J. Phys. Chem. C 125 (2021) 28157–28161.
[10] M. Attrash, M.K. Kuntumalla, S. Michaelson, A. Hoffman, Nitrogen terminated diamond (111) by RF(N2) plasma – chemical states, thermal stability and structural properties, Surf. Sci. 703 (2021) 121741.
[11] Y. Zheng, A. Hoffman, K. Huang, Atomistic insight into nitrogen-terminated Diamond(001) Surfaces by the adsorption of N, NH, and NH2: a density functional theory study, Langmuir 37 (2021) 6248–6256.
[12] A. Stacey, M. O'Donnell Kane, J.-P. Chou, A. Schenk, A. Tadich, N. Dontschuk, J. Cervenka, C. Pakes, A. Gali, A. Hoffman, S. Prawer, Nitrogen terminated diamond, Adv. Mater. Interfaces 2 (2015) 1500079.
[13] R. Jones, J.P. Goss, H. Pinto, D.W. Palmer, Diffusion of nitrogen in diamond and the formation of A-centres, Diamond Relat. Mater. 53 (2015) 35–39.
[14] C.L.A. Lamont, J. Wilkes, Attenuation length of electrons in self-assembled monolayers of n-alkanethiols on gold, Langmuir 15 (1999) 2037–2042.
[15] H. Borchert, S. Haubold, M. Haase, H. Weller, C. McGinley, M. Riedler, T. Möller, Investigation of ZnS passivated InP nanocrystals by XPS, Nano Lett. 2 (2002) 151–154.
[16] M. Zier, S. Oswald, R. Reiche, K. Wetzig, Non-destructive depth profile analysis using synchrotron radiation excited XPS, Microchim. Acta 156 (2006) 99–101.
[17] S.V. Merzlikin, N.N. Tolkachev, T. Strunskus, G. Witte, T. Glogowski, C. Wöll, W. Grünert, Resolving the depth coordinate in photoelectron spectroscopy – Comparison of excitation energy variation vs. angular-resolved XPS for the analysis of a self-assembled monolayer model system, Surf. Sci. 602 (2008) 755–767.
[18] R.G. Haverkamp, A.T. Marshall, B.C.C. Cowie, Energy resolved XPS depth profile of (IrO2, RuO2, Sb2O5, SnO2) electrocatalyst powder to reveal core-shell nanoparticle structure, Surf. Interface Anal. 43 (2011) 847–855.
[19] M. Gawek, S. Madkour, P. Szymoniak, J. Radnik, A. Schönhals, Energy dependent XPS measurements on thin films of a poly(vinyl methyl ether)/polystyrene blend concentration profile on a nanometer resolution to understand the behavior of nanofilms, Soft Matter 17 (2021) 6985–6994.
[20] M. Brzhezinskaya, E.A. Belenkov, V.A. Greshnyakov, G.E. Yalovega, I.O. Bashkin, New aspects in the study of carbon-hydrogen interaction in hydrogenated carbon nanotubes for energy storage applications, J. Alloys Compd. 792 (2019) 713–720.
[21] M.M. Brzhezinskaya, V.E. Muradyan, N.A. Vinogradov, A.B. Preobrajenski, W. Gudat, A.S. Vinogradov, Electronic structure of fluorinated multiwalled carbon nanotubes studied using x-ray absorption and photoelectron spectroscopy, Phys. Rev. B 79 (2009) 155439.
[22] R. Graupner, F. Maier, J. Ristein, L. Ley, C. Jung, High-resolution surface-sensitive C 1s core-level spectra of clean and hydrogen-terminated diamond (100) and (111) surfaces, Phys. Rev. B 57 (1998) 12397–12409.
[23] M. Fischer, M. Chandran, R. Akhvlediani, A. Hoffman, Interplay between adhesion and interfacial properties of diamond films deposited on WC-10%Co substrates using a CrN interlayer, Diamond Relat. Mater. 70 (2016) 167–172.
[24] A. Nefedov, C. Wöll, Advanced applications of NEXAFS spectroscopy for functionalized Surfaces, in: G. Bracco, B. Holst (Eds.), Surface Science Techniques, Springer, Berlin Heidelberg, Berlin, Heidelberg, 2013, pp. 277–303.
[25] M. Sobaszek, M. Brzhezinskaya, A. Olejnik, V. Mortet, M. Alam, M. Sawczak, M. Ficek, M. Gazda, Z. Weiss, R. Bogdanowicz, Highly occupied Surface states at deuterium-grown boron-doped diamond Interfaces for efficient photoelectrochemistry, Small 19 (2023) 2208265.
[26] Z. Shpilman, I. Gouzman, E. Grossman, L. Shen, T.K. Minton, J.T. Paci, G.C. Schatz, R. Akhvlediani, A. Hoffman, Oxidation and etching of CVD diamond by thermal and hyperthermal atomic oxygen, J. Phys. Chem. C 114 (2010) 18996–19003.
[27] R. Larciprete, P. Lacovig, S. Gardonio, A. Baraldi, S. Lizzit, Atomic oxygen on graphite: chemical Characterization and thermal reduction, J. Phys. Chem. C 116 (2012) 9900–9908.
[28] M.K. Kuntumalla, A. Hoffman, Influence of different nitrogen plasmas exposures of H-diamond (100) Surfaces on ambient oxygen adsorption, nitrogen bonding, and thermal stability studied by X-ray photoelectron spectroscopy, Phys. Status Solidi A n/a (2023) 2300319.
[29] M.P. Seah, W.A. Dench, Quantitative electron spectroscopy of surfaces: a standard data base for electron inelastic mean free paths in solids, Surf. Interface Anal. 1 (1979) 2–11.
[30] A.K. Schenk, K.J. Rietwyk, A. Tadich, A. Stacey, L. Ley, C.I. Pakes, High resolution core level spectroscopy of hydrogen-terminated (1 0 0) diamond, J. Phys.: Condens. Matter 28 (2016) 305001.
[31] F.N. Li, R. Akhvlediani, M.K. Kuntumalla, A. Hoffman, Oxygen bonding configurations and defects on differently oxidized diamond surfaces studied by high resolution electron energy loss spectroscopy and X-ray photoelectron spectroscopy measurements, Appl. Surf. Sci. 465 (2019) 313–319.
[32] S. Sangtawesin, B.L. Dwyer, S. Srinivasan, J.J. Allred, L.V.H. Rodgers, K. De Greve, A. Stacey, N. Dontschuk, K.M. O'Donnell, D. Hu, D.A. Evans, C. Jaye, D.A. Fischer, M.L. Markham, D.J. Twitchen, H. Park, M.D. Lukin, N.P. de Leon, Origins of diamond Surface noise probed by correlating single-spin measurements with Surface spectroscopy, Phys. Rev. X 9 (2019) 031052.
[33] A.V. Okotrub, L.G. Bulusheva, V.L. Kuznetsov, A.V. Gusel'nikov, A.L. Chuvilin, Electronic state of nanodiamond/graphite interfaces, Appl. Phys. A 81 (2005) 393–398.
[34] F.C.I. Catalan, L.T. Anh, J. Oh, E. Kazuma, N. Hayazawa, N. Ikemiya, N. Kamoshida, Y. Tateyama, Y. Einaga, Y. Kim, Localized graphitization on diamond Surface as a manifestation of dopants, Adv. Mater. 33 (2021) 2103250.
[35] M. Fischer, M.K. Kuntumalla, G. Gani, A. Hoffman, Entrapment and thermal stability of low energy argon implanted into diamond studied by in-situ X-ray photoelectron spectroscopy and thermal programmed desorption, Appl. Surf. Sci. 615 (2023) 156358.

[36] T. Petit, J.-C. Arnault, H.A. Girard, M. Sennour, T.-Y. Kang, C.-L. Cheng, P. Bergonzo, Oxygen hole doping of nanodiamond, Nanoscale 4 (2012) 6792–6799.
[37] A. Hoffman, G. Comtet, L. Hellner, G. Dujardin, M. Petravic, Surface near-edge x-ray adsorption fine structure of hydrogenated diamond films and Di(100) surfaces studied by H+ and H− ion desorption, Appl. Phys. Lett. 73 (1998) 1152–1154.
[38] Z. Shpilman, I. Gouzman, T.K. Minton, L. Shen, A. Stacey, J. Orwa, S. Prawer, B.C. C. Cowie, A. Hoffman, A near edge X-ray absorption fine structure study of oxidized single crystal and polycrystalline diamond surfaces, Diamond Relat. Mater. 45 (2014) 20–27.
[39] A. Laikhtman, I. Gouzman, A. Hoffman, G. Comtet, L. Hellner, G. Dujardin, Sensitivity of near-edge x-ray absorption fine structure spectroscopy to ion beam damage in diamond films, J. Appl. Phys. 86 (1999) 4192–4198.
[40] A. Laikhtman, A. Hoffman, Interaction of thermally activated and molecular oxygen with hydrogenated polycrystalline diamond surfaces studied by synchrotron radiation techniques, Surf. Sci. 522 (2003) L1–L8.
[41] K.C. Prince, R. Richter, M. de Simone, M. Alagia, M. Coreno, Near edge X-ray absorption spectra of some small polyatomic molecules, J. Phys. Chem. A 107 (2003) 1955–1963.
[42] J.F. Morar, F.J. Himpsel, G. Hollinger, G. Hughes, J.L. Jordan, Observation of a C-1s Core exciton in diamond, Phys. Rev. Lett. 54 (1985) 1960–1963.
[43] A. Chemin, I. Levine, M. Rusu, R. Vaujour, P. Knittel, P. Reinke, K. Hinrichs, T. Unold, T. Dittrich, T. Petit, Surface-mediated Charge transfer of photogenerated Carriers in diamond, Small Methods 7 (2023) 2300423.